

Document downloaded from:

<http://hdl.handle.net/10251/105514>

This paper must be cited as:

Rizescu, C.; Podolean, I.; Cojocaru, B.; Parvulescu, VI.; Coman, SM.; Albero-Sancho, J.; García Gómez, H. (2017). RuCl₃ supported on N-doped graphene as reusable catalyst for one-step glucose oxidation to succinic acid. *ChemCatChem*. 9(17):3314-3321.
doi:10.1002/cctc.201700383



The final publication is available at

<https://doi.org/10.1002/cctc.201700383>

Copyright John Wiley & Sons

Additional Information

RuCl₃ supported on N-doped graphene as reusable catalyst for one-step glucose oxidation to succinic acid

Cristina Rizescu,^[a] Iunia Podolean,^[a] Bogdan Cojocaru,^[a] Vasile I. Parvulescu,^{*[a]} Simona M. Coman,^[a] Josep Albero,^[b] Hermenegildo Garcia^{*[b]}

Abstract: Impregnation of RuCl₃ on N-doped graphenes results in the formation of well-dispersed, small ruthenium oxyhydroxide nanoparticles supported on N-doped graphene that may exhibit high selectivity (87 %) for the conversion of glucose into succinic acid under wet oxidation conditions (160 °C, 18 atm O₂ pressure). Ruthenium loading and N atom distribution on graphene influence the catalytic activity, the best performing catalyst having 1 wt% Ru loading on a graphene having a large population of graphenic N atoms. The high catalytic selectivity to succinic acid has been correlated with the presence of small ruthenium nanoparticles. The present catalyst improves the best one previously reported, since it does not require the continuous addition of an excess of amine to reach high succinic acid selectivity and reusability.

Introduction

Green chemistry has a continued interest in developing highly efficient, easily recoverable and recyclable catalysts.^{[[1]]} In this respect, due to the high specific surface area, high dispersability in liquid media, strong adsorption capacity and excellent mechanical and electronic properties, graphenes (Gs) are currently attracting considerable interest as supports for active metals.^{[[2]]} Besides their intrinsic properties, the physical and chemical properties of Gs can be tailored in a significant extent by doping with heteroatoms such as N, P, B, S, or functional moieties like NH₂-groups, etc.^{[[3]]} The presence of these heteroatoms modulate the strength and mode of interaction between G and the metal NPs.^{[[2b, 4]]}

On the other hand, nowadays, there is also a high interest in the use of biomass as renewable feedstock and one promising strategy is the catalytic aerobic oxidation of raw materials to valuable organic molecules.^{[[5]]} In this context, not long ago we developed an efficient heterogeneous Ru(III)-based catalyst for the oxidation of levulinic acid to succinic acid (SA) (selectivity to SA 96-98% for levulinic acid conversion of 59-79%).^{[[6]]} However, the one-pot, selective catalytic oxidation of C6 sugar molecules

(ie, glucose, fructose) to valuable dicarboxylic acids appears to be more challenging and appealing due to the higher availability of C6 sugars as starting materials.^{[[7]]}

In general oxidation of glucose leads to complex mixtures. Thus, wet air oxidation (WO) of glucose, at 110-140 °C in neutral solution yields a wide range of reaction products in inadequate low selectivity, including gluconic and glucaric acids, glucosone, 5-ketogluconic and arabonic acids, and various degradation products with four or less number of carbon atoms.^{[[8]]} Interestingly enough, the WO of glucose, with an unexpected yield of 62.7% in SA, was achieved at 180 °C in neutral solution using a supported ruthenium (III) catalyst to enhance the selectivity.^{[[9]]} In the presence of Ru(III), the catalytic WO (CWO) of glucose affords SA, along lesser amounts of carboxylic acids with a lower molecular mass, such as lactic, glycolic and glyceric acid.^{[[9]]} Addition of an excess of amines, such as *n*-butylamine, to the catalytic system (*n*-butylamine/Ru molar ratio of 12.5) improved the catalytic performance of the supported ruthenium (III) catalyst (yield to SA of 87.5% for a total conversion of glucose) and continued addition of *n*-butylamine in each run allowed reuse of Ru(III) catalyst for several cycles.^{[[9]]} This remarkable and unexpected influence of the presence of *n*-butylamine was explained taking into consideration several effects caused by the presence of amine, such as: i) favoring the desorption of the carboxylic acids generated in the oxidation that otherwise would be strongly adsorbed to the Ru(III) species, ii) increasing the stability of the Ru nanoparticles (NPs) minimizing their growth by acting as ligands, and iii) stabilizing Ru(IV) species that are the catalytically active species.

Considering the current importance of SA as monomer of polyesters and polyamides, as well as the economic attractiveness of converting glucose directly to SA by oxygen in aqueous medium, it would be important to improve the stability of Ru (III) catalyst, particularly to find alternatives to the continued addition of an excess of amine. With the aim to further improve the Ru (III) system for this valuable one-pot synthesis of SA from glucose, it will be shown in this work that N-containing Gs as supports of Ru species is an efficient catalysts for the selective CWO of glucose to SA and it constitutes a green alternative to the use of molecular amines that become decomposed under the conditions of CWO. In the new heterogeneous catalytic system described here, the N atoms coordinating to Ru(III) are not a molecular additive, but a constitutive part of the N-doped G acting as support of Ru(III) complexes, allowing easy separation and recycling of the catalyst without the need of continued addition of an excess of ligand to maintain the catalytic activity. Nitrogen is directly incorporated on the G sheet during the preparation of the material. In addition, the use of such Ru/N-doped G catalysts makes also possible decreasing the temperature of the CWO in

[a] C. Rizescu, I. Podolean, B. Cojocaru, V. I. Parvulescu, S. M. Coman
Department of Organic Chemistry, Biochemistry and Catalysis
Faculty of Chemistry, University of Bucharest
Bdul Regina Elisabeta 4-12, Bucharest 030016, Romania
E-mail: vasile.parvulescu@chimie.unibuc.ro

[b] J. Albero, H. Garcia
Instituto Universitario de Tecnología Química CSIC-UPV
Universitat Politècnica de Valencia
Av. De los Naranjos s/n, 46022 Valencia, Spain
E-mail: hgarcia@qim.upv.es

Supporting information for this article is given via a link at the end of the document.

comparison with the previously reported *n*-butylamine modified Ru-catalytic system.^{[[9]]} Thus, considering that Ru (III) supported on N-doped Gs is a truly reusable catalyst, the system described here is advantageous respect to the previously reported homogeneous Ru(III) complex.

Results and Discussion

Catalysts Characterization

Two types of N-doped Gs were prepared and used as supports of RuCl₃. In one N-doped G materials, graphene oxide (GO) was the starting material and it was submitted to treatment with NH₃ solutions of different concentrations. It is known that this solvothermal process leads to a simultaneous incorporation of N atoms on the G sheet while GO reduction is taking place,^{[[10]]} resulting in three NH₂-rGO(x) (x indicates the weight percentage of N) samples. A second type of N-doped G was obtained by pyrolysis of chitosan at 900 °C under inert atmosphere. Chitosan is a natural polysaccharide of glucosamine obtained by deacetylation of chitin and acts as source of carbon and nitrogen. It has been reported that pyrolysis of this biopolymer at temperatures above 900 °C results in N-doped G (N-G).^{[[11]]} Table 1 lists the N-doped Gs used in the present study as supports and their N content.

Table 1. List of N-doped Gs used in this study with their corresponding N-content and its distribution among different N types.

Samples	N content (%)	N distribution (%), XPS		
		Quaternary (399.8 eV)	Pyridinic (398.1 eV)	Amine (399.8 eV)
N-G	4.6	72	28	-
NH ₂ -rGO(3.8)	3.8	100	-	-
NH ₂ -rGO(5.3)	5.3	64	36	-
NH ₂ -rGO(8.5)	8.5	14	36	50

After support preparation, they were impregnated with RuCl₃ solutions in order to obtain 1 or 5 wt% Ru supported N-containing G catalysts (Ru/N-containing G) and the materials were characterized as dry powders by XRD, XPS, Raman and microscopy techniques.

Except for one sample as it will be commented below, all the diffraction peaks recorded in the XRD patterns presented in Figure 1 for Ru/N-containing G samples as dry powders

correspond to the G support, without appearing any peak attributable to any Ru phase.

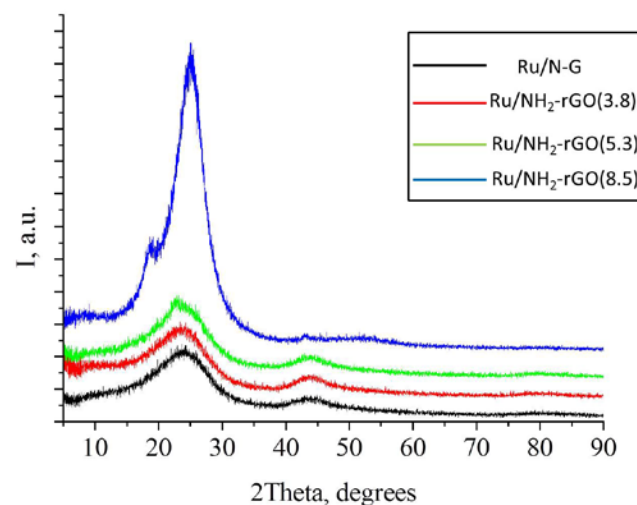


Figure 1. XRD patterns of the series of RuCl₃ catalysts supported on various modified Gs at 5% loading. From top to bottom: Ru/N-G (black), Ru/NH₂-rGO (3.8) (red), Ru/NH₂-rGO (5.3) (green), and Ru/NH₂-rGO (8.5) (blue).

Thus, the two broad lines at 2θ angle values of about 25° and 43° are attributable to the (002) and (100) plane reflections of Gs (Figure 1). Apart of typical lines at 25.2 and 43.2°, the XRD pattern of Ru/NH₂-rGO(8.5) catalyst displays plane reflections centered at 18.7 and 52.4°, respectively. The last peak has been indexed as the γ-band and, although its origin has not been totally explained, it has been previously observed and attributed by Hirsch et al. to short-range order of aromatic lamellae.^{[[12]]} In accordance with reports of Knights and co-workers^{[[13]]} the pronounced (002) lines at around 23-25.0° could be assigned to the layer-to-layer distances of the powdered G material with loose π stacking of the layers, while the very broad (100) line at around 43° could be attributed to the main dimension in the plane of a two-dimensional layer structure. Therefore, the d-spacing was calculated by applying the Bragg's law: $d = \lambda / 2 \sin \theta$ (where λ is the X-ray wavelength, 1.542 Å, and θ is the Bragg angle), while the main size of the crystallite along c-axis (evaluated from the width of the (002) diffraction line, denoted τ₀₀₂) and the main dimension in the plane of a two-dimensional layer structure (evaluated from the width of the (100) diffraction line, denoted τ₁₀₀) were estimated using the Scherrer equation: $\tau = K\lambda / \beta \cos \theta$ (where K is the dimensionless shape factor that is considered as 1.84 for τ₁₀₀ and 0.89 for τ₀₀₂ calculation; λ is the X-ray wavelength, 1.542 Å; β is full width at half maximum intensity in radians, and θ is the Bragg angle).^{[[14]]} If each parallel layer consists of N layers, τ₀₀₂ for a parallel layer group is defined as:^{[[15]]}

$$\tau_{002} = (N - 1)d_{002} \text{ or } N = (\tau_{002} + d_{002}) / d_{002}$$

The detailed X-ray crystalline parameters obtained as indicated above are collected in Table 2. Although it should be remarked that the information provided by XRD refers to Ru/N-containing Gs as solid powders and not dispersed in aqueous phase, they serve to illustrate that even under dry conditions, the stacking is limited to a few layers. It can be assumed that this stacking will decrease or will be maintained upon sonication in the aqueous reaction medium.

Table 2. Structural parameters estimated from X-ray diffraction for the series of G-supported RuCl₃ at 5 wt% samples as powders.

Sample	XRD position of the (002) plane, d-spacing and number of layers				
	θ , plane (002)	d-spacing Å	τ_{100} , Å	τ_{002} , Å	Number of layers
Ru/N-G	11.95	3.72	24.6	7.8	3.1
Ru/NH ₂ -rGO (3.8)	11.85	3.75	30.1	9.1	3.4
Ru/NH ₂ -rGO (5.3)	11.55	3.85	26.6	9.1	3.4
Ru/NH ₂ -rGO (8.5)	12.0 (9.35)	3.71 (4.74)	94.9	15.1	5.1

Only in the case of the Ru/NH₂-rGO (8.5) sample at 5 wt% Ru loading, a diffraction line at 52.4° was additionally recorded in the XRD pattern. This peak can be attributed to an amorphous ruthenium oxide phase, giving a valuable information about the state of Ru on the materials. For all the other samples, no peaks attributable to ruthenium species could be detected, indicating that for most of the Ru/N-doped Gs ruthenium particles should be present as very small, well dispersed crystallites on the modified G sheets. This will agree with TEM images as commented below.

XPS afforded information about the electronic state of the constitutive elements of the G-based Ru samples. Figure 2 presents the experimental high-resolution N1s peaks and the best deconvolution to its individual components, while Table 1 summarizes the results. Each N type has a characteristic binding energy (BE) value in XPS: pyridinic N (398.1 eV), pyrrolic N (399.8 eV) and quaternary N (400.4 -401.3 eV) [16] and, accordingly, it is possible to estimate the percentage of each type of N atom from the best deconvolution of the experimental XPS N_{1s} peak to individual components. In the present case, deconvolution of the XPS N_{1s} peaks indicates that no component with BE corresponding to pyridine N-oxide (~402.8 eV) is present in significant proportion in the investigated samples.

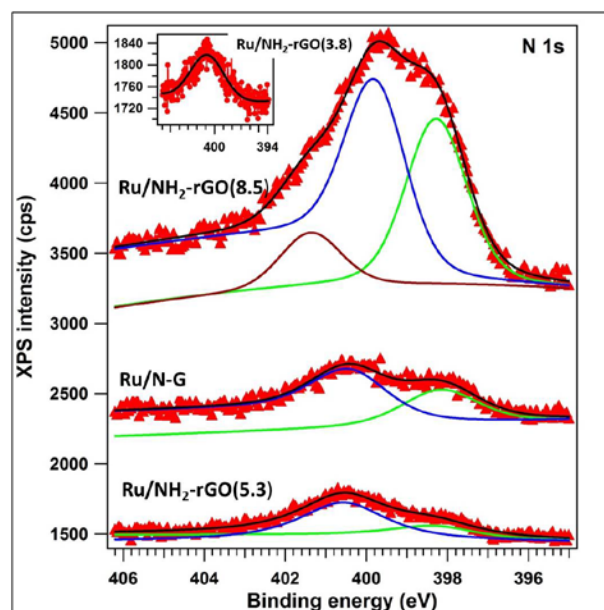


Figure 2. XPS core-level spectra for the N_{1s} region of the G-based Ru samples at 5 wt% loading.

While quaternary N (pyridinium or graphitic sp² hybridized N replacing C atoms in the hexagonal network of G) was present in all analyzed samples (Figure 2 and Table 1), amine N (sp³ N hybridized), [17] was identified only for the Ru/NH₂-rGO (8.5) sample (ie the sample containing the largest N content). Ru/NH₂-rGO (8.5) should contain 50% of sp³ hybridized N atoms (Table 1). The large difference of the quaternary N peak position in Ru/NH₂-rGO (8.5) sample (401.3 eV versus 400.4 eV in the other samples, Figure 2) should correspond to a different nitrogen loading and different neighbor atoms. [17]

Quite interesting, the higher the amount of N atoms in G, the smaller the proportion of quaternary N was. Accordingly, in Ru/NH₂-rGO (3.8) most of the N present in the sample exists in quaternary configuration, while in Ru/NH₂-rGO (8.5) only 14 % from the total N exhibit a quaternary configuration and the majority are sp³ N atoms corresponding to the amino groups. Except for Ru/NH₂-rGO (3.8), pyridinic N (N atoms bonded to two C atoms at the edges or defects of the G sheet, contributing with one p electron to the π system) should be present according to XPS N_{1s} deconvolution in all samples in quite similar proportion (28-36%), irrespective of the N atom concentration.

Doping with N also shifts the BE of the C1s level (not shown). [16b] For investigated G-based Ru samples at 5 wt% Ru loading, a sharp peak at around 284.5 eV corresponds to the graphene sp² carbons (Figure S11 in the supporting information). Higher energy components correspond to sp² and sp³ carbon atoms in different C-O bonding configurations, including simple C-O bonds, carbonyls C=O bonds and carboxylates (O=C-O) at about 286, 287 and 289 eV, respectively. [18] Since, in the present case the samples contain also N atoms, its presence will also influence the BE of N-coordinated C atoms. Sheng et al. [18]

attributed the BE at 285.8 and 287.5 eV to the sp^2 (C=N) and sp^3 (C-N) carbon atoms, respectively.

For Ru/N-G and Ru/NH₂-rGO (5.3) catalysts, analysis of the Ru_{3p} level indicated a dominant peak centered at 463.3 eV (Figure 3 a), which can be attributed to the RuO₂ phase.^{[[19]]} The Ru_{3p} XPS spectrum of 5wt%Ru/NH₂-rGO (3.8) showed a BE centered at 462.2 eV, and its deconvolution revealed as well the existence of the RuO₂ phase. Notably, the component at 462.2 eV suggests that the incorporated N atoms on the G framework transfer electron density to the Ru active sites, decreasing the BE value. Analysis of the O_{1s} level (Figure 3 b) clearly shows a component at 531.5 eV that corresponds to RuO₂. The XPS data of Ru_{3p} and N_{1s} support the conclusion that Ru is present on the surface of N-containing Gs as small, well dispersed Ru(IV) oxyhydroxide and/or RuO₂ particles, the latter being also in agreement with the XRD of Ru/NH₂-rGO(8.5) that is the only case in which a peak for Ru species was recorded.

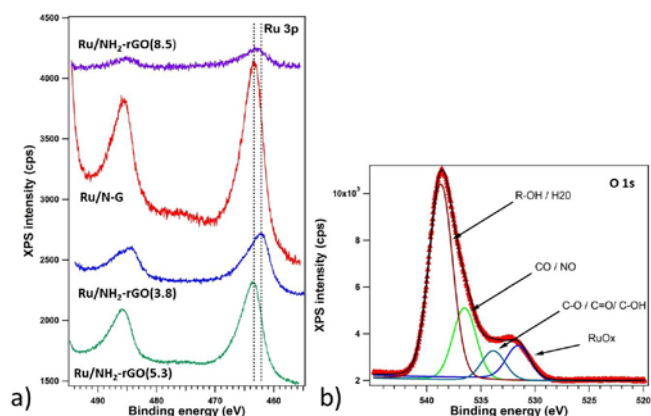


Figure 3. XPS core-level spectra for the Ru_{3p} region of the Ru/N-containing G samples (a) and best deconvolution XPS core-level spectra for the O_{1s} region of the Ru/NH₂-rGO (3.8) sample (b).

TEM images of Ru/NH₂-rGO(3.8) show the expected 2D morphology for graphene with light contrast and the presence of very small Ru NPs of size below 1 nm. Statistical determination of the particle size indicates that the average diameter of the fresh sample is Ru/NH₂-rGO(3.8) 0.74±0.15 nm. Figure 4 presents selected images of this sample before and after reaction. The small size for Ru NPs is in agreement with the previous comments about the absence in XRD of Ru/NH₂-rGO(3.8) of any diffraction peak attributable to Ru species.

Thermoprogrammed desorption (TPD) of CO₂ after preadsorption of this gas at room temperature can provide a quantitative indication of the number and strength distribution of basic sites for both Ru/N-G and Ru/NH₂-rGO samples. Figure 5 shows the CO₂ desorption profiles as a function of temperature. The total basic site densities (CO₂ mmol/g) were measured by integration of TPD curves and are summarized in Table 3. The TPD profiles of modified G-containing Ru samples were deconvoluted taking three desorption peaks: a low temperature

peak at 100 °C, a middle-temperature peak in the range 230-250 °C and a high-temperature peak between 340 and 370 °C.

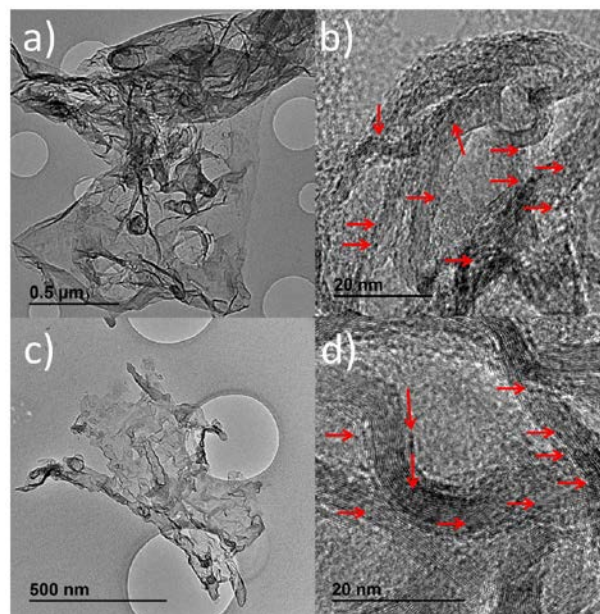


Figure 4. TEM images at two different magnifications of Ru/NH₂-rGO(3.8) before (a and b) and after its use in four consecutive (c and d) reactions. Images (a) and (c) correspond to a general view of the sample before and after reaction, respectively. (b) and (d) corresponds to high-resolution images of (a) and (c) images, respectively, where some Ru NPs have been highlighted with red arrows.

The assignment of the CO₂ desorption peaks was done based on the different types of nitrogen species determined by N_{1s} peak deconvolution in the XPS spectra (see Figure 2 and Table 1). Thus, the weak sites were attributed to the interaction of CO₂ with pyridinic N, medium strength sites with quaternary N and strong sites to the interaction of CO₂ with ruthenium oxyhydroxide species. This assignment was also supported by comparison of the TPD profiles of the samples containing Ru with those of the N-doped G supports lacking Ru that did not exhibit the high temperature desorption peak, indicating that the sites of stronger basicity are associated to the presence of ruthenium deposition in the samples (Table 3).

TPD measurements by CO₂ provide evidence that the basic strength and density of Ru oxyhydroxy NPs depends on the interaction with the N-doped G support, the strong basic sites on Ru being particularly notable for the samples containing the highest N contents and being absent for the Ru/N-G and Ru/NH₂-rGO (3.8) that will be catalytically the most active samples.

There are examples in the literature showing that the presence of graphenic N atoms on G can influence the charge distribution of the neighbor carbon atoms resulting in a zone on G that is especially suited for binding of active metal atoms and metal NPs.^{[[20]]}

In addition, it has been calculated and determined experimentally that N-doped carbon can donate electrons to the anchored metallic species, favoring the reduced states of the metals.^{[[4b, 21]]}

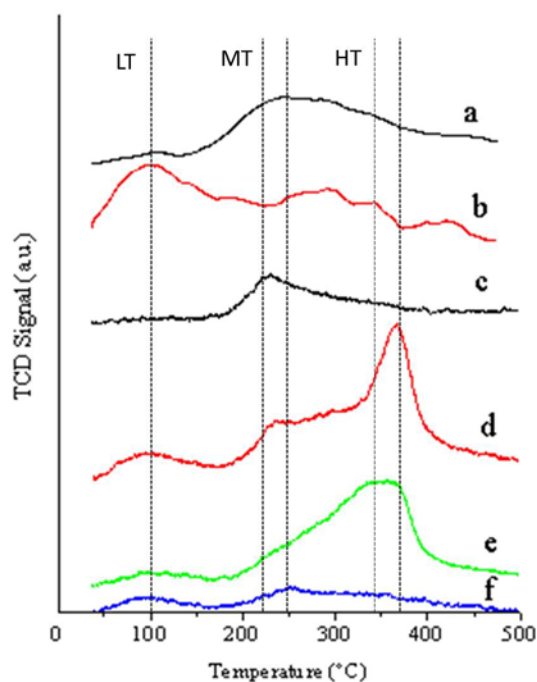


Figure 5. CO₂-TPD profiles of the N-containing Gs without and at 5 wt% Ru loading: a. NH₂-rGO (3.8); b. NH₂-rGO (5.3); c. Ru/NH₂-rGO (3.8) sample; d. Ru/NH₂-rGO (5.3) sample; e. Ru/NH₂-rGO (8.5) sample, and f. Ru/N-G sample. Dotted lines correspond to the low temperature (LT), middle temperature (MT) and high temperature (HT) regions.

Table 3. Basic strength distribution for Ru/N-containing Gs at 5 wt% Ru loading.

Sample	Base sites density, mmoles/g			Total
	Weak (pyridinic)	Medium (quaternary)	Strong (Ru(IV) oxyhydroxide)	
Ru/N-G	0.05	0.20	-	0.25
Ru/NH ₂ -rGO (3.8)	-	0.17	-	0.17
Ru/NH ₂ -rGO (5.3)	0.02	0.005	0.175	0.20
Ru/NH ₂ -rGO (8.5)	0.015	0.15	0.180	0.21

Thus, in line with these precedents it is proposed that in the present case graphenic nitrogen atoms grafted on G should contribute, through the creation of an *activation region* in which a strong interaction of G with the ruthenium precursor occurs, to the stabilization of small, well dispersed Ru(IV) oxyhydroxide and/or RuO₂ particles that do not exhibit basicity.

Catalytic activity

As commented in the introduction, the aim of the present study is to develop a heterogeneous, reusable and selective catalytic system for the valuable one-pot synthesis of SA from glucose based on supporting of Ru species on N-doped Gs. This strategy may provide a greener alternative to the reported cationic Ru (III) anchored on aminopropylsilica coated magnetic NP (Ru@MNP), whose main limitation was the requirement of continued addition of an excess of primary amines in order to reuse the catalyst.^{[[9]]}

Under the WO conditions, hydroxy and hydroperoxy radicals are formed via reduction of oxygen and dissociation and oxidation of water, resulting also in the generation of a concentration of hydrogen peroxide.^{[[22]]} These radicals, together with the free oxygen, can attack at the reducing end group of glucose (ie, aldehyde group), resulting in the opening of the glycosidic ring and the formation of carboxylic acids. Indeed, in the absence of any catalytic species, experiments proved that the WO of glucose at 180 °C and 10 atm O₂ using water as solvent led to a complex mixture of various low molecular acids (as lactic, glyceric and glycolic acids among others) along significant amounts of aldonic acids. Under these conditions in the absence of catalyst, glucose conversion was below 12 % and SA selectivity was below 3 %. Control experiments using N-doped Gs in the absence of Ru showed that the selectivity to SA at 1.5 h under the previous conditions is also below 5 %.

Glucose conversion and SA selectivity increased dramatically when the WO was carried out in the presence of Ru/N-doped G as catalysts. Table 4 provides a summary of the activity data under various conditions for the samples under study. As it can be seen there, the presence of Ru at 5 wt% loading on N-containing G improved both the conversion of glucose (from 20 to 71.4%) and the selectivity to SA (from 3.6 to 21.8%) with respect to those of the blank control or in the presence of N-doped Gs. However, the performance of G supported Ru catalysts was still poor compared to the activity and selectivity of other heterogeneous Ru catalysts.^{[[9]]} Decreasing the reaction temperature to 160 °C, increasing the O₂ pressure to 18 atm, resulted at longer time also in complete glucose conversions and the selectivity to SA values were much higher (52.8-62.1%), although still far from 87 % reported for Ru@MNP in the presence of an excess of butylamine.^{[[9]]}

To further optimize the performance of Ru NPs deposited on N-doped G, the catalytic activity of samples with lower Ru loading (1 wt%) was also evaluated. While at 160 °C and 18 atm O₂, glucose conversion was complete irrespective of Ru 1 or 5 wt% loading, the highest selectivity in SA was achieved using catalysts with smaller Ru loadings, reaching 81-87 % for 1 wt% in comparison to the 62-69 % SA selectivity values for 5 wt% Ru

(Table 4, entries 1-8). Other products observed were C3 and C2 carboxylic acids, particularly hydroxypropionic and lactic acids. In one of the conditions, the combined selectivity to SA and hydroxypropionic acid was over 95% at total glucose conversion what is really a remarkable value considering typical complex reaction mixtures formed in WO.

The influence of Ru loading on the selectivity of the CWO reaction can be interpreted considering that higher loadings should lead to larger, less-active Ru particles that should favor glucose decomposition to small carboxylic acids.

This explanation is in agreement with the catalytic activity of Ru/NH₂-rGO (8.5) at 5 wt% Ru loading containing larger Ru oxide NPs even detectable by XRD that is the poorest performing catalyst of all the set of samples. In contrast, it is expected that small Ru particles as those shown in Figure 4 for Ru/NH₂-rGO (3.8) should exhibit a larger catalytic activity, influencing in a larger extent the course of glucose WO. As result of the high catalytic activity of Ru/doped G, a higher proportion of SA that is a product not formed in significant percentage in the non-catalytic oxidation pathways, as deduced from the results of the blank controls, will be formed. In fact, as

commented below regarding the reaction mechanism proposal, the formation of SA should involve other steps besides radical oxidation, like deoxygenation and hydrogenation that do require the presence of an active catalyst to occur.

As commented above when discussing the influence of Ru loading on the catalytic acidity, the N-containing G as support plays a role controlling the catalytic activity of supported ruthenium oxyhydroxide NPs. To confirm the role of nitrogen-doping on G in achieving these high performances, independent tests were carried out with an analogous catalyst having the same loading of Ru (1 wt%), but deposited on a nitrogen-free reduced graphene oxide (rGO) obtained similarly to NH₂-rGO, but without NH₃ in the hydrothermal reduction (Table 4, entry 9. See Figure SI2 and SI3 for the corresponding XPS).

Table 4. Catalytic performance of N-containing G supporting Ru in the catalytic WO of glucose.^a

Entry	Catalyst	Conversion (%)	Selectivity, % ^b				
			SA (C4)	LA (C3)	HPA (C3)	GlyA (C3)	GA (C2)
1	Ru/NH ₂ -rGO (3.8) 1wt%	100	87.0	1.9	8.4	0	1.7
2	Ru/NH ₂ -rGO (3.8) 5 wt%	100	69.1	8.8	10.2	0	11.8
3	Ru/N-G 1 wt%	100	83.2	2.6	9.2	0	3.5
4	Ru/N-G 5 wt%	100	65.0	13.8	11.4	5.2	5.0
5	Ru/NH ₂ -rGO (5.3) 1 wt%	100	81.3	5.1	9.0	0	3.0
6	Ru/NH ₂ -rGO (5.3) 5 wt%	100	62.3	10.2	15.3	0	8.4
7	Ru/NH ₂ -rGO (8.5) 5 wt%	100	52.8	12.8	6.8	1.1	25.3
8	Ru/NH ₂ -rGO (3.8) 5wt% ^c	71.4	21.8	< 3 %	0	0	< 5%
9	Ru/G 1 wt%	100	-	-	-	3.3	23.4
10	N-G ^a	11.3	< 5%	0	< 3%	7	17
11	Blank ^a	< 12%	< 3%	0	< 3%	< 3%	< 5%

^a Reaction conditions: 0.5 mmoles glucose, 0.025 g catalyst, 10 ml H₂O, 160 °C, 18 atm O₂, 20 h. ^b The difference to 100% in selectivity corresponds to lactones, hexoses and glucose isomers. SA – succinic acid; LA – lactic acid; HPA – 3-hydroxypropionic acid; GlyA – glyceric acid; GA – glycolic acid. ^c 180 °C, 10 atm O₂, 1.5 h.

The optimal N-containing G supports are those having the largest proportion of graphenic N atoms. Figure 6 presents the correlation between the percentage of graphenic N atoms on G

and SA selectivity. SA selectivity also follows an inverse trend with the CO₂ TPD measurements of the catalyst, those samples exhibiting higher density of strong basic sites due to large ruthenium NPs being the less selective towards SA.

Stability of the Ru/NH₂-rGO (3.8) catalyst at 1 wt% Ru loading was confirmed by recovering the material after the reaction and reusing in four consecutive runs (Figure SI4).

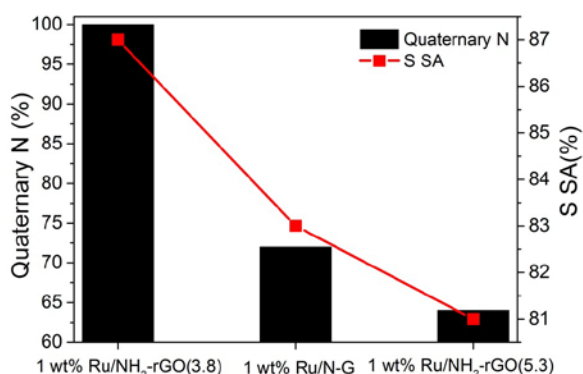


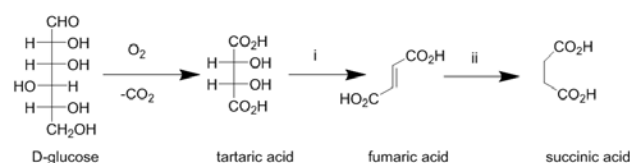
Figure 6. Variation of the selectivity to SA as a function of the type and content of N atoms for N-containing G supported Ru at 1 wt% Ru loading.

It was observed that the activity for glucose conversion and the selectivity towards SA do not change in four consecutive uses. Moreover, analysis of the four times used Ru/NH₂-rGO (3.8) sample showed that the Ru content was maintained. Analysis of the particle size distribution of Ru NPs by HRTEM of the four times reused Ru/NH₂-rGO (3.8) sample showed some increase in the average particle size and in the dispersion of the size distribution (see Figure 4). However, these variations of average particle size from 0.93±0.26 nm of the four times used with respect to the 0.74±0.15 nm of the fresh sample were relatively minor and, apparently at this level they are not reflected in the catalytic performance.

In addition, XPS analysis of the four times used 1 wt% Ru/NH₂-rGO (3.8) was also performed and compared with the data of the fresh sample. Table SI1 summarizes the relevant XPS data. The 1 wt% Ru/NH₂-rGO (3.8) catalyst showed notable variations in the C1s peak that indicate the occurrence of an extensive oxidation (Figure SI1). These changes in the C1s are understandable considering the conditions of CWO. It was, however, somehow, surprising the significant decrease revealed by XPS in the O/Ru ratio of the four times used 1 wt% Ru/NH₂-rGO (3.8) respect to the fresh sample (Table SI1). This variation suggests that the oxygen content of the RuO₂ NPs decreases along the reactions, something that contrasts with the previously commented increase in the oxygen coordination of the C atoms. This oxygen depletion on Ru atoms is probably caused by the reducing power of glucose and polyols that can act as hydrogenating reagents through hydrogen transfer mechanism and is indicative of the role of Ru as CWO catalyst. The binding energy of the Ru3p peak indicates, however, that the Ru(IV) oxidation state is preserved in the reaction.

Concerning the reaction pathways involved in the formation of SA, the previous findings that ruthenium oxide NPs are able to promote the deoxygenation of tartaric acid, as well as hydrogen transfer from polyols to fumaric acid has allowed us to propose the mechanism shown in Scheme 1. In this

mechanism the key intermediates will be tartaric acid formed by oxidative decarboxylation from glucose and fumaric acids. None of these C₄ acids are detected in significant amount in the reaction mixtures, probably due their fast conversion into SA. This reaction mechanism is compatible with the observation that O/Ru decreases during the CWO, making possible for Ru to promote the oxidative deoxygenation of tartaric acid into fumaric acid that is a process that would not occur in the absence of Ru catalyst (step i in Scheme 1) and that been observed already for Ru@MNP. Hydrogenation of fumaric acid would occur, on the other hand, through hydrogen transfer from polyols that is a process that is generally catalyzed by Ru.



Scheme 1. Proposed intermediates in the conversion of glucose into succinic acid.

Conclusions

In conclusion, the conversion of glucose into succinic acid in water by oxygen can be promoted at 160 °C and 18 atm. O₂ pressure with a selectivity close to 90 % by using ruthenium supported on N-containing graphene as catalyst without the addition of an excess of amine as co-catalyst. The Ru/N-doped G is reusable at least in four consecutive runs without changes in activity and selectivity of the sample, although characterization of the used catalysts indicates an increase in the oxygen coordination on graphenic C atoms and a decrease in the oxygen coordination around Ru. Characterization data shows that the predominant Ru species present initially on the catalyst are ruthenium oxyhydroxide NPs of particle size below 1 nm. It has been observed that the performance of the Ru/N-doped G catalyst depends on Ru loading and the N atom distribution, being the best performing samples those having small size and homogeneously distributed ruthenium NPs as consequence of the low Ru loading and the presence of graphenic N atoms on G. The present findings constitute a step forward towards the development of catalyst to promote the selective conversion of glucose into succinic acid.

Experimental Section

Catalysts preparation

Two different types of N-doped G were used in the present study. In one case N-doped G was prepared by pyrolysis of chitosan and subsequent exfoliation of the carbon residue, as previously reported.^[23] In brief, low molecular weight chitosan (Sigma Aldrich) was pyrolyzed as powder under argon atmosphere using the following temperature program for the

oven: annealing at 200 °C for 2 h and, then, heating at 10 °C/min up to 900 °C, maintaining this flow.

A second type of N-doped Gs were prepared by dispersing 100 mg of GO, previously obtained by Hummers method, in 40 mL of ethylene glycol upon sonication at 700 W for 3 h and subsequent addition of increasing aqueous ammonia concentrations (5, 10, 20 %) as nitrogen source. The dark brown solutions were transferred to Teflon-lined autoclave and heated at 175 °C under autogenous pressure for 16 h. The resulting black solid was filtered and washed with distilled water until neutral pH was obtained. Finally, the NH₂-doped Gs were dried at 60 °C for 24 h.

Suspensions of the corresponding N-doped Gs were obtained by sonicating the black graphitic powders at 700 W for 1 h in the aqueous and removing the non-exfoliable particles by centrifugation.

Impregnation of the N- and NH₂-doped Gs with a RuCl₃ solution at basic pH (pH=13) was performed by adding 2 g of N-containing G to an aqueous solution (400 mL distilled water) of hydrated ruthenium (III) chloride (Aldrich) in amounts corresponding to a final concentration of 1 wt% and 5 wt% Ru. The pH was adjusted at 13 with the aid of a 1 M aqueous solution of NaOH. The slurry was maintained under stirring at 25 °C for 24 h. The solid was then separated by centrifugation, washed twice with distilled water and acetone, dried under vacuum and calcined at 400 °C, for 4 h.

Catalysts characterization

HRTEM images were recorded in a JEOL JEM 2100F under accelerating voltage of 200kV. Samples were prepared by applying one drop of the suspended material in ethanol onto a carbon-coated copper TEM grid, and allowing them to dry at room temperature.

X-ray diffraction (XRD) patterns were recorded with a Shimadzu XRD 7000 diffractometer using a CuK_α radiation source ($\lambda = 1.542 \text{ \AA}$) at a scan rate of 1 ° min⁻¹ in the range from 5 to 70 °.

XPS measurements were performed in a Specs instrument using Al K_α monochromated radiation ($h\nu = 1486.7 \text{ eV}$) of an X-ray gun, operating at 300 W (12 kV/25 mA) power. A flood gun with electron acceleration at 1 eV and electron current of 100 μA was used in order to avoid charge effects. Photoelectron energy was recorded at normal angle emission by using a Phoibos 150 analyzer, operating with pass energy of 30 eV. The XP spectra were fitted by using Voigt profiles combined with their primitive functions, for inelastic backgrounds.^{[[24]]} The Gaussian width of all lines and thresholds do not differ considerably from one spectrum to another, being always in the range of 2 eV.

CO₂-TPD measurements were carried out using the AutoChem II 2920 station. The samples (30-50 mg), placed in a U-shaped quartz reactor with an inner diameter of 0.5 cm, were pre-treated under He (Purity 5.0, from Linde) at 100 °C for 1 h, and then exposed to a flow of CO₂ (from SIAD) for 1 h. After that, the sample was purged with a flow of He (50 mL min⁻¹) for 20 min at 25 °C in order to remove the weakly adsorbed CO₂ species. TPD measurement was then started, with a heating rate of 10 °C min⁻¹ till 700 °C. The desorbed products were analyzed with a TC detector. The CO₂ desorbed, expressed as mmols of CO₂ per gram of catalyst, was determined using a calibration curve.

Catalytic tests

Activity tests in batch mode were carried out by adding 25 mg of catalysts to a solution of 90 mg (0.5 mmols) glucose in 10 mL water. After closing, the reactor was pressurized between 10 and 18 bars with molecular oxygen and heated up to 160-180 °C, under stirring (1200 rpm), for 1-20 h. After reaction, oxygen was released, the catalyst was separated by centrifugation and the products were recovered from the residue after removal of H₂O under reduced pressure. The recovered products were silylated, diluted with 1 mL of toluene and analyzed by GC-FID chromatography (GC-Shimadzu apparatus). The identification of the products was made using a GC-MS Carlo Erba Instruments QMD 1000 equipped with a Factor Four VF-5HT column.

Acknowledgements

Financial support by the Spanish Ministry of Economy and Competitiveness (Severo Ochoa, Grapas and CTQ2015-69563-CO2-R1) and by the Generalitat Valenciana (Prometeo 2013-014) is gratefully acknowledged. J.A. also thanks the Universitat Politècnica de Valencia for a postdoctoral scholarship. Prof. Simona M. Coman kindly acknowledges UEFISCDI for financial support (project PN-II-PT-PCCA-2013-4-1090, Nr. 44/2014).

Keywords: N-doped graphene • ruthenium • oxidation • glucose • succinic acid

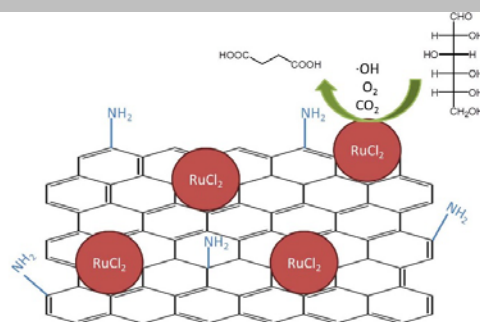
- [1] a) P. T. Anastas, M. M. Kirchoff, *Acc. Chem. Res.* **2002**, *35*, 686-694; b) J. H. Clark, *Green Chem.* **1999**, *1*, 1-8.
- [2] a) J. Alberio, H. Garcia, *J. Mol. Catal. A: Chem.* **2015**, *408*, 296-309; b) S. Navalon, A. Dhakshinamoorthy, M. Alvaro, H. Garcia, *Coord. Chem. Rev.* **2016**, *312*, 99-148.
- [3] a) H. Liu, Y. Liu, D. Zhu, *J. Mater. Chem.* **2011**, *21*, 3335-3345; b) H. Wang, T. Maiyalagan, X. Wang, *ACS Catal.* **2012**, *2*, 781-794; c) Z. Yang, Z. Yao, G. Li, G. Fang, H. Nie, Z. Liu, X. Zhou, X. a. Chen, S. Huang, *ACS Nano* **2012**, *6*, 205-211.
- [4] a) X. Fan, G. Zhang, F. Zhang, *Chem. Soc. Rev.* **2015**, *44*, 3023-3035; b) D. He, Y. Jiang, H. Lv, M. Pan, S. Mu, *Appl. Catal. B: Environ.* **2013**, *132-133*, 379-388; c) Z. Li, J. Liu, Z. Huang, Y. Yang, C. Xia, F. Li, *ACS Catal.* **2013**, *3*, 839-845; d) P. Trogadas, T. F. Fuller, P. Strasser, *Carbon* **2014**, *75*, 5-42; e) X. Xie, J. Long, J. Xu, L. Chen, Y. Wang, Z. Zhang, X. Wang, *RSC Adv.* **2012**, *2*, 12438-12446.
- [5] A. Corma, S. Iborra, A. Velty, *Chem. Rev.* **2007**, *107*, 2411-2502.
- [6] I. Podolean, V. Kuncser, N. Gheorghe, D. Macovei, V. I. Parvulescu, S. M. Coman, *Green Chem.* **2013**, *15*, 3077-3082.
- [7] P. Gallezot, *Catal. Today* **1997**, *37*, 405-418.
- [8] J. M. Skaates, B. A. Briggs, R. A. Lamparter, C. R. Baillod, *Can. J. Chem. Eng.* **1981**, *59*, 517-521.
- [9] I. Podolean, C. Rizescu, C. Bala, L. Rotariu, V. I. Parvulescu, S. M. Coman, H. Garcia, *ChemSusChem* **2016**, *9*, 2307-2311.
- [10] D. Long, W. Li, L. Ling, J. Miyawaki, I. Mochida, S.-H. Yoon, *Langmuir* **2010**, *26*, 16096-16102.
- [11] A. Primo, E. Sánchez, J. M. Delgado, H. García, *Carbon* **2014**, *68*, 777-783.
- [12] L. Cartz, R. Diamond, P. B. Hirsch, *Nature* **1956**, *177*, 500-502.
- [13] D. Geng, S. Yang, Y. Zhang, J. Yang, J. Liu, R. Li, T.-K. Sham, X. Sun, S. Ye, S. Knights, *Appl. Surf. Sci.* **2011**, *257*, 9193-9198.
- [14] O. O. Sonibare, T. Haeger, S. F. Foley, *Energy* **2010**, *35*, 5347-5353.
- [15] H. P. Klug, E. A. Leroy, *X-Ray Diffraction Procedures for Polycrystalline and Amorphous Materials*, John Wiley & Sons, New-York, **1974**.
- [16] a) T. C. Drage, K. M. Smith, C. Pevida, A. Arenillas, C. E. Snape, *Energy Procedia* **2009**, *1*, 881-884; b) J. Duan, S. Chen, M. Jaroniec, S. Z. Qiao, *ACS Catal.* **2015**, *5*, 5207-5234.

- [17] C. P. Ewels, M. Glerup, *J. Nanosci. Nanotechnol.* **2005**, *5*, 1345-1363.
- [18] Z.-H. Sheng, L. Shao, J.-J. Chen, W.-J. Bao, F.-B. Wang, X.-H. Xia, *ACS Nano* **2011**, *5*, 4350-4358.
- [19] S. Armenise, L. Roldán, Y. Marco, A. Monzón, E. García-Bordejé, *J. Phys. Chem. C* **2012**, *116*, 26385-26395.
- [20] L. Zhang, Z. Xia, *J. Phys. Chem. C* **2011**, *115*, 11170-11176.
- [21] a) T. Alonso-Lanza, A. Ayuela, F. Aguilera-Granja, *ChemPhysChem* **2015**, *16*, 3700-3710; b) S. Lee, Y.-C. Chung, *J. Solid State Chem.* **2013**, *205*, 160-164; c) J. Liang, M. Hassan, D. Zhu, L. Guo, X. Bo, *J. Colloid Interface Sci.* **2017**, *490*, 576-586; d) N. Park, S. Moon; e) R. Czerw, M. Terrones, J. C. Charlier, X. Blase, B. Foley, R. Kamalakaran, N. Grobert, H. Terrones, D. Tekleab, P. M. Ajayan, W. Blau, M. Rühle, D. L. Carroll, *Nano Lett.* **2001**, *1*, 457-460.
- [22] S. Roy, M. Vashishtha, A. K. Saroha, *J. Eng. Sci. Technol. Rev.* **2010**, *3*, 95-107.
- [23] A. Primo, P. Atienzar, E. Sanchez, J. M. Delgado, H. Garcia, *Chem. Commun.* **2012**, *48*, 9254-9256.
- [24] C. M. Teodorescu, J. M. Esteva, R. C. Karnatak, A. El Afif, *Nucl. Instrum. Meth. A* **1994**, *345*, 141-147.

Entry for the Table of Contents

FULL PAPER

Glucose is converted in 90 % selectivity to succinic acid under catalytic wet oxidation conditions using ruthenium supported on N-containing graphene as catalyst without the addition of amines as co-catalyst.



Cristina RIZESCU, Iunia Podolean, Bogdan Cojocaru, Vasile I. Parvulescu, Simona M. Coman, Josep Albero, Hermenegildo Garcia**

Page No. – Page No.

RuCl₃ supported on N-doped graphene as reusable catalyst for one-step glucose oxidation to succinic acid